Viscosity of disordered Dirac electrons

Weiwei Chen and W. Zhu[*]

School of Science, Westlake University, 18 Shilongshan Road, Hangzhou 310024, China
and Institute of Natural Sciences, Westlake Institute for Advanced Study, 18 Shilongshan Road, Hangzhou 310024, China

Rejuvenation of hydrodynamic transport in solids provides a new window to study the collective motion of electrons, where electrons behave like a viscous fluid akin to classical liquids. So far the discussion on the fate of hydrodynamic electronics in the presence of disorder scattering is largely phenomenological, and a systematical study is still lacking. Here we investigate the hydrodynamic properties of Dirac electron fluid in graphene from a microscopic viewpoint. We present strong evidence that, due to frequent electron-hole collisions, the shear viscosity can be enhanced by electron-disorder scattering in the low-energy region, which is in sharp contrast to the common sense of traditional Fermi liquids. Moreover, we clarify that the anomalous behavior of Dirac electron fluid can be also revealed by the dynamic and magneto-hydrodynamics. Therefore, our paper demonstrates the exotic landscape of hydrodynamic electronics in graphene, and presents experimentally relevant responses to quantify the effects of electronic viscosity.

I. INTRODUCTION

Hydrodynamic behavior of electrons in solids has been predicted for decades [1], but only in the recent years has it become a reality in two-dimensional materials, where many signatures of viscous electron flows have been probed, such as negative local resistance [2,3], superballistic flow [4–6], current vortices [7–9], Poiseuille flow [10,11], Hall viscosity [12], and violation of the Wiedemann-Franz law [13,14]. Generally speaking, to maximize hydrodynamic effects in experiment, so far there are two main roads. One is to seek a material in which momentum relaxing effects (e.g., electron-phonon scattering) are greatly suppressed. In this respect, graphene becomes a promising candidate to observe hydrodynamic phenomena, due to its extremely stiffness. The other way is to create inhomogeneous electron flows moving through artificial constriction geometry such as a narrow slit [2], where hydrodynamic behavior is generally expected. Beyond the above two ways, an ongoing quest is to find more mechanism that can amplify the hydrodynamic effect in electron fluids, which is not only conceptually important but also practically relevant for experiment.

Most of existing studies on hydrodynamic effect focus on the electron-electron collisions [15–17], and theoretical modeling of viscous electron flow is usually based on the simulation of Navier-Stokes equations [17–19], where the prevalence of imperfection like disorder is usually overlooked. One plausible reason is that disorder is always expected to disrupt collective motions by introducing a momentum-relaxing collisions [20,21]. To date a systematic study of disorder effect on hydrodynamic phenomena in experimentally relevant two-dimensional materials is still lacking. On the other hand, it has been known that disorder profoundly impacts carrier transport in graphene. One novel example is the observation of minimum conductivity in graphene [22], originating from impurity assisted resonant tunneling of massless Dirac fermions [23–25]. Hence, with this fact on hand, it is natural to ask to what extent hydrodynamic phenomena could be promoted or symbiotic coexistence in disordered Dirac electron fluids. In this paper, we investigate the disorder effect on Dirac electron liquid in graphene. Counterintuitively, we discover an enhancement of viscosity for Dirac electron fluid, which endows the graphene system with interesting, yet mostly unexplored, static and dynamic hydrodynamic behavior.

To fully understand the disorder effect on hydrodynamic electronics, we systematically study the shear η_s and Hall η_H viscosities in disordered graphene, using analytic and numerical methods. We consider both static and dynamic situations, with or without an external magnetic field. First of all, we analytically identify the static η_s shear viscosity enclosing an additional term inversely proportional to the quasiparticle relaxation time in the undoped graphene, which implies η_s is enhanced by disorder near the Dirac point. In addition, the shear viscosity around the Dirac point can be further enhanced by an external magnetic field. These findings are in stark contrast to those found in the conventional two-dimensional ordinary electron gas (2DEG) [26], suggesting the importance of the inherent electron-hole coherence around the Dirac point of graphene. (For a detailed comparison please see Table I.) Moreover, these anomalous behaviors also leave fingerprints in the dynamic and magneto-hydrodynamics. Away from charge neutrality, the viscosity coefficients tend to agree with those of Fermi liquids. All these findings are highly relevant to the on-going experiments on graphene, calling for detailed studies of hydrodynamic electronics of Dirac fluid.

*zhuwei@westlake.edu.cn

TABLE I. Analytic results of static shear (η_s) and Hall (η_H) viscosity of disordered graphene in the absence of magnetic field $B = 0$ and presence of perpendicular magnetic field $\boldsymbol{B} = B\hat{z}$. E is the Fermi energy, ρ is the density of states, τ is the quasiparticle relaxation time, N is index of Landau level, A is disorder scattering parameter, and ε is the distance between the Fermi energy and the nearest Landau level center. In 2DEG, $\tilde{\omega}_c = \frac{eB}{m}$ is the cyclotron frequency. In graphene, $\tilde{\omega}_c = \frac{eB}{|E|/v_f^2}$ is effective cyclotron frequency. They are equivalent by introducing effective mass $m = |E|/v_f^2$ in graphene. "Overlapped" and "Well separated" are the regions divided by $\tilde{\omega}_c \tau \lesssim 1$ and $\tilde{\omega}_c \tau \gg 1$.

	η_s in the case $B = 0$	η_s in the case $\boldsymbol{B} = B\hat{z}$		η_H in the case of $\boldsymbol{B} = B\hat{z}$	
		Overlapped	Well separated	Overlapped	Well separated
2DEG	$\frac{1}{2}E^2\rho\tau$ [26,28]	$\frac{1}{2}\frac{E^2\rho\tau}{1+4(\tilde{\omega}_c\tau)^2}$ [26,27]	$\frac{N^2\hbar}{8\pi^2 l_B^2}(1-2A\varepsilon^2)$ [26]	$\frac{\rho\tilde{\omega}_c\tau^2 E^2}{1+4\tilde{\omega}_c^2\tau^2}$ [26–28]	$\frac{N^2\hbar}{8\pi l_B^2} - \frac{1}{4\tilde{\omega}_c}\frac{\rho E^2}{1+4\tilde{\omega}_c^2\tau^2}$ [26]
Graphene	$\frac{1}{8}E^2\rho\tau + \frac{3}{32}\frac{\hbar^2\rho}{\tau}$	$\frac{1}{8}\frac{E^2\rho\tau}{1+4\tilde{\omega}_c^2\tau^2} + \frac{\hbar^2}{32\tau}\rho\frac{3+16\tilde{\omega}_c^2\tau^2}{1+4\tilde{\omega}_c^2\tau^2}$	$\frac{(N^2+\delta_{N,0})\hbar}{2\pi^2 l_B^2}(1-2A\varepsilon^2)$	$\frac{1}{4}\frac{\rho\tilde{\omega}_c\tau^2 E^2}{1+4\tilde{\omega}_c^2\tau^2}$	$\frac{\text{sgn}(E)(2N^2+2N+1)\hbar}{4\pi l_B^2} - \frac{1}{16\tilde{\omega}_c}\frac{\rho E^2}{1+4\tilde{\omega}_c^2\tau^2}$

A. Summary of results

The main results of this paper are summarized below. First of all, we obtain the analytical expression of static shear viscosity of graphene as (details in Sec. III A),

$$\eta_s(E) = \frac{1}{8}E^2\rho\tau + \frac{3}{32}\frac{\hbar^2\rho}{\tau}.$$

The first term has the same origin with that in 2DEG, but the second term does not. The second term is inversely proportional to the quasiparticle relaxation time τ and implies the viscosity will be enhanced by disorder potential in the low-energy region where the first term is suppressed. This is contrary to popular belief about classical fluids and ordinary metals, where impurities usually tends to destroy collective behavior of particles.

Second, our result implies that the shear viscosity of clean graphene at the Dirac point is zero rather than infinity. It is essentially related to the zero density of states ($\rho = 0$) in this condition even though the electron-electron interaction is neglected.

Third, the shear viscosity in the ordinal metal decreases with magnetic field due to the correction for the cyclotron motion, we find the shear viscosity closed to the Dirac point can be enhanced by the magnetic field denoted as (details in Sec. III A)

$$\eta_s(E \to 0) = \frac{3A}{8\pi^2\hbar^2 v_f^2}\left[E_c e^{-A/2} + \frac{\hbar v_f^2}{E_c e^{-A/2}}eB\right]^2.$$

This unexpected result is also reminiscent of disorder assisted electron-hole collisions around the Dirac point and puts forth suggestions for future experimental detection of electron fluids.

Fourth, the dynamic shear viscosity differs significantly in the following two regions: electron-hole (e-h) coherence-dominated region ($E \approx 0 \ll \Omega$) and electron-electron (e-e) coherence-dominated region ($0 < \Omega \ll E$) (details in Sec. IV A),

$$\eta_s(\Omega) = \begin{cases} \frac{\Omega^2}{16\hbar v_f^2}\left(\frac{1}{2} + \frac{16}{15A}\right), & E \approx 0 \ll \Omega \\ \frac{AE^2}{2\pi^2\hbar v_f^2}\left(\frac{\pi^2}{A^2} + \frac{E^2}{A^2\Omega^2+4E^2}\right), & 0 < \Omega \ll E \end{cases}.$$

The dynamic shear viscosity has opposite dependence on the frequency in these two regions. Additionally, when e-h coherence predominates, the dependence of dynamic shear viscosity on disorder strength is monotonically increasing, while when e-e coherence predominates, the dependence of dynamic of dynamic shear viscosity on disorder strength becomes complicated.

Fifth, based on the evaluations of dynamic shear and Hall viscosity in the presence of magnetic field, assuming good separation of Landau levels, we find that they are both determined by the state transitions between Landau levels, $E_{ns} \leftrightarrow E_{ms'}$, where the level indices satisfy $|m - n| = 2$ and there is no restriction on s and s'. Moreover, the interband transition counterparts $E_{n,-} \to E_{n+2,+}$ and $E_{n+2,-} \to E_{n,+}$ contribute the same to dynamic shear viscosity, they cancel each other in dynamic Hall viscosity (details in Secs. IV A and IV B).

Sixth, in our extensive calculations, the Hall viscosity of Dirac electrons is in line with that in 2DEG. It reflects the topological origin [29] of Hall viscosity that should be independent on the details such as electron dispersion.

Finally, we make a detailed comparison with 2DEG, as shown in Table I.

B. Outline

The paper is organized as follows. In the Sec. II, we establish the formalism of the viscosity in graphene. We review the definition of shear and Hall viscosity in Sec. II A, and derive the strain generators and symmetric stress tensor of Dirac fermion to establish the structure of the viscosity tensor from first principles without relying on any phenomenological assumptions in Sec. II B. Then, the viscosity is obtained based on the linear response between strain rate tensor and stress tensor and expressed by the Kubo formula in terms of Green's function in Sec. II C. In Sec. II D, we present the eigenbasis of the pure system and derive the self-energy in short-range disorder. The specific calculations of static and dynamic viscosities are displayed in Sec. III and Sec. IV. In Sec. III A, we present analytical and numerical solutions of the static shear viscosity of graphene in the absence of magnetic field and the presence of the perpendicular magnetic field. In Sec. III B, we present analytical and numerical solutions of static Hall viscosity of graphene with perpendicular magnetic field. In Sec. IV A and Sec. IV B, we present the corresponding dynamic shear and Hall viscosities. Finally, we discuss the results obtained and offer some perspectives in Sec. V.

II. METHODS

A. Definition of shear and Hall viscosity

The viscosity, which relates the viscous stress in a fluid to the rate of change of a deformation (i.e., strain rate), is defined in a homogeneous Newtonian fluid by the following relation [30]:

$$\tau_{ij} = \sum_{kl} \eta_{ij,kl} \frac{\partial \lambda_{kl}}{\partial t}, \tag{1}$$

where $\eta_{ij,kl}$ is the viscosity tensor, τ_{ij} is the stress tensor, $\lambda_{kl} = \frac{1}{2}(\frac{\partial u_k}{\partial x_l} + \frac{\partial u_l}{\partial x_k})$ is the symmetric strain tensor, and u_i is the deformation displacement along i direction. In an isotropic system, τ_{ij} is also symmetric so that η is symmetric under $i \leftrightarrow j$ and $k \leftrightarrow l$. Thus, η can be divided into symmetric and antisymmetric parts with respect to interchanging the first with the second pair of indices. Based on these features, the viscosity tensor of a two dimensional isotropic system is characterized in a natural basis $\eta = \sum \eta_{ab} \sigma_a \otimes \sigma_b$ ($a, b = 0, x, z$) by three coefficients [28,30–32],

$$\begin{aligned}
\eta_{ij,kl} &= \zeta \sigma_0 \otimes \sigma_0 + \eta_s (\sigma_z \otimes \sigma_z + \sigma_x \otimes \sigma_x) \\
&\quad + \eta_H (\sigma_z \otimes \sigma_x - \sigma_x \otimes \sigma_z) \\
&= \begin{pmatrix}
\begin{pmatrix} \zeta + \eta_s & \eta_H \\ \eta_H & \zeta - \eta_s \end{pmatrix}_{kl} & \begin{pmatrix} -\eta_H & \eta_s \\ \eta_s & \eta_H \end{pmatrix}_{kl} \\
\begin{pmatrix} -\eta_H & \eta_s \\ \eta_s & \eta_H \end{pmatrix}_{kl} & \begin{pmatrix} \zeta - \eta_s & -\eta_H \\ -\eta_H & \zeta + \eta_s \end{pmatrix}_{kl}
\end{pmatrix}_{ij}
\end{aligned} \tag{2}$$

where the symmetric components under the exchange ($ij \leftrightarrow kl$), ζ and η_s denote bulk viscosity and shear viscosity, and the antisymmetric components under the exchange ($ij \leftrightarrow kl$), η_H denotes Hall viscosity. In an incompressible fluid ($\frac{\partial \lambda_{ii}}{\partial t} = 0$), the stress becomes independent of ζ. Thus, the incompressible and isotropic fluids in two dimensions are characterized by two coefficients one for the even part η_s and one for the odd part η_H. η_s contributes to dissipation of energy, so it is also called dissipative viscosity. η_H is dissipationless and only exist when time reversal symmetry is broken.

B. Strain deformation and stress tensor

In the following, we derive the expression of the stress tensor in two ways. On the one hand, we associate the spatial strain transformation of the system with the unitary transformation of the Hamiltonian and derive the stress in quantum-mechanical theory. On the other hand, we simulate graphene by a symmetric $2 + 1$ dimensional Dirac field and obtain the stress tensor based on the Noether's theorem combining symmetrization procedure of Belinfante.

a. Quantum-mechanical theory of stress. In quantum-mechanical theory, the stress is considered to be an intrinsic property of the quantum-mechanical ground state of matter response to deformation [33], so we start from using the unitary transformation in Hilbert space to describe the deformation. The Hamiltonian of the charge carriers of graphene near the half filling is described by a two-dimensional massless Dirac particles with the speed of light replaced by v_f,

$$H = v_f \boldsymbol{\sigma} \cdot \boldsymbol{p} \tag{3}$$

where $\boldsymbol{\sigma} = (\sigma_x, \sigma_y)$ are the Pauli matrices of pseudospin. In the presence of magnetic field, the Hamiltonian is changed by $\boldsymbol{p} \to \boldsymbol{\Pi} = \boldsymbol{p} + e\boldsymbol{A}$.

The infinitesimal spatial deformation can be described as

$$x_i \to x_i' = x_i + u_i(\boldsymbol{x}) = u_{0,i} + \frac{\partial u_i}{\partial x_j} x_j + o(x^2) \tag{4}$$

where $u_{0,i}$ corresponds to the translation so that is ignored here, and the repeated indices are summed in all cases. Then the matrix of deformation transformation ($\boldsymbol{x}' = \Lambda \boldsymbol{x}$) can be derived as [34]

$$\Lambda = 1 + \frac{1}{2}\lambda_{ij}(x_j \partial_i + x_i \partial_j) - \frac{1}{4} r_{ij}(x_i \partial_j - x_j \partial_i) \tag{5}$$

where we introduced strain tensor λ_{ij} and rotation tensor r_{ij},

$$\lambda_{ij} = \frac{1}{2}\left(\frac{\partial u_i}{\partial x_j} + \frac{\partial u_j}{\partial x_i}\right), \quad r_{ij} = \frac{\partial u_i}{\partial x_j} - \frac{\partial u_j}{\partial x_i}. \tag{6}$$

It is noticed that the strain tensor is symmetric ($\lambda_{ij} = \lambda_{ji}$) and the rotation tensor is antisymmetric ($r_{ij} = -r_{ji}$). Based on this infinitesimal transformation, we can define two generators, strain transformation generator $\mathcal{J}_{ij}$ and rotation transformation generator L_{ij}, which is the well-known angular momentum,

$$\mathcal{J}_{ij} = -\frac{1}{2}(x_i p_j + x_j p_i), \qquad L_{ij} = x_i p_j - x_j p_i. \tag{7}$$

The strain transformation generator is symmetric ($\mathcal{J}_{ij} = \mathcal{J}_{ji}$) and the rotation transformation generator is antisymmetric ($L_{ij} = -L_{ji}$). Thus, one can parametrize the representation of spatial strain transformation $\mathcal{S}(\lambda)$ in terms of the strain transformation generator as

$$\mathcal{S}(\lambda) = e^{-i\lambda_{ij}\mathcal{J}_{ij}/\hbar}. \tag{8}$$

Then, the deformed Hamiltonian is obtained by using time-dependent unitary operator $\mathcal{S}[\lambda(t)]$ [35],

$$H_\lambda(t) = \mathcal{S}H\mathcal{S}^{-1} + i\hbar\frac{\partial \mathcal{S}}{\partial t}\mathcal{S}^{-1} = H - \frac{i\lambda_{ij}}{\hbar}[\mathcal{J}_{ij}, H] + \frac{\partial \lambda_{ij}}{\partial t}\mathcal{J}_{ij}. \tag{9}$$

Thus one can obtain the integral stress tensor by the fundamental thermodynamic relation for deformed bodies [31,36,37]

$$T_{ij} = \int d\boldsymbol{r}\,\tau_{ij} = -\frac{\partial H_\lambda}{\partial \lambda_{ij}} = \frac{i}{\hbar}[\mathcal{J}_{ij}, H]. \tag{10}$$

Substituting the Hamiltonian equation (3) into the above equation and performing Fourier transformation, the symmetric stress tensor is obtained as

$$T_{ij} = \frac{v_f}{2}(\sigma_i p_j + \sigma_j p_i), \tag{11}$$

which does not contain the effect from disorder potential since that one strains the electron liquid rather than the host materials [26].

In the presence of magnetic field, the spatial strain transformation should couple a gauge transformation $\mathcal{S}(\lambda) \to \mathcal{S}(\lambda)e^{-\frac{ie}{\hbar}\xi}$. Thus, the Eq. (10) becomes $T_{ij} \to \frac{i}{\hbar}e^{-\frac{ie}{\hbar}\xi}[\mathcal{J}_{ij}, H]e^{\frac{ie}{\hbar}\xi}$. It is obvious that the stress tensor under magnetic field is obtained by $\boldsymbol{p} \to \boldsymbol{\Pi} = \boldsymbol{p} + e\boldsymbol{A}$.

Above, we obtained the stress tensor based on the thermodynamics of deformation, in fact, Eq. (10) is equal to the definition in a metric compatible Riemannian manifold $T_{\mu\nu} = 2\frac{1}{\sqrt{|g|}}\frac{\delta S}{\delta g^{\mu\nu}}$ [38], where the small deformations strain tensor is replaced by the fundamental metric tensor, which have the relation $\lambda_{ij} = \frac{1}{2}(g_{ij} - \delta_{ij})$. δ_{ij} plays the role of the fundamental metric tensor for undeformed region whose geometry corresponds to a flat Euclidean space [39].

Another thing worth noting is that for the same stress tensor T_{ij}, the strain transformation generator $\mathcal{J}_{ij}$ that satisfies the relation, $T_{ij} = \frac{i}{\hbar}[\mathcal{J}_{ij}, H]$, is not unique. In previous papers [40,41], it was established that a strain transformation generator including strain transformations in pseudospin of graphene as $\mathcal{J}'_{ij} = -\frac{1}{2}\{x_i, p_j\} + \frac{i\hbar}{8}[\sigma_i, \sigma_j]$, and they acquired the same stress tensor as Eq. (11). The similarity between $\mathcal{J}_{ij}$ and $\mathcal{J}'_{ij}$ is that they are both symmetric [42]. The latter is closer to the symmetrization procedure of Belinfante in field theory, which we will simply derive in $2 + 1$ dimensional Dirac field.

b. Belinfante stress-energy-momentum tensor in field theory. The symmetric stress tensor can also be arrived from Belinfante stress-energy-momentum tensor in field theory. We start with a symmetric Lagrangian density of a $2 + 1$ dimensional Dirac field,

$$\mathcal{L} = \frac{i}{2}\hbar v_f \bar{\psi}\bar{\sigma}^{\mu}(\overrightarrow{\partial}_{\mu} - \overleftarrow{\partial}_{\mu})\psi, \quad (12)$$

where $\bar{\psi} = \psi^{\dagger}\sigma_z$ is adjoint of the field ψ, $D_{\nu} \equiv (\partial_{v_f t}, \nabla)$ is the covariant derivation in time-space coordinate, the Dirac matrices are chosen as

$$\bar{\sigma}^0 = \sigma_z; \quad \bar{\sigma}^1 = i\sigma_y; \quad \bar{\sigma}^2 = -i\sigma_x; \quad (13)$$

which satisfy Clifford algebra $\{\bar{\sigma}^{\mu}, \bar{\sigma}^{\nu}\} = 2g^{\mu\nu}$.

Based on the Noether's theorem, one can obtain the canonical stress-energy-momentum tensor [38],

$$\tau^{\mu\nu} = \frac{\partial \mathcal{L}}{\partial(\partial_{\mu}\psi)}\partial^{\nu}\psi + \partial^{\nu}\bar{\psi}\frac{\partial \mathcal{L}}{\partial(\partial_{\mu}\bar{\psi})} - g^{\mu\nu}\mathcal{L}$$

$$= \frac{i}{2}\hbar v_f \bar{\psi}\bar{\sigma}^{\mu}(\overrightarrow{\partial}^{\nu} - \overleftarrow{\partial}^{\nu})\psi. \quad (14)$$

By adding the divergence of a Belinfante tensor $B^{\alpha\mu\nu}$ antisymmetric in the first two indices ($B^{\alpha\mu\nu} = -B^{\mu\alpha\nu}$),

$$B^{\alpha\mu\nu} = \frac{1}{8}\hbar v_f \bar{\psi}\left\{\bar{\sigma}^{\alpha}, \frac{i}{2}[\bar{\sigma}^{\mu}, \bar{\sigma}^{\nu}]\right\}\psi, \quad (15)$$

one can obtain the Belinfante stress-energy-momentum tensor as

$$\tau^{\mu\nu}_B = T^{\mu\nu} + \partial_{\alpha}B^{\alpha\mu\nu}$$

$$= \frac{i}{4}\hbar v_f \bar{\psi}[\bar{\sigma}^{\mu}(\overrightarrow{\partial}^{\nu} - \overleftarrow{\partial}^{\nu}) + \bar{\sigma}^{\nu}(\overrightarrow{\partial}^{\mu} - \overleftarrow{\partial}^{\mu})]\psi. \quad (16)$$

Here, τ^{00}_B represents the energy density, τ^{0i}_B the momentum density (or energy flux density), and τ^{ij}_B the stress tensor. Since this stress tensor is derived for the Lagrangian density, the integral form of τ^{ij}_B is consistent with Eq. (11).

C. Kubo formula of viscosity

Since we have got the expression of the deformed Hamiltonian and stress tensor, the viscosity defined in Eq. (1) can be evaluated by the linear response theory [31],

$$\langle T_{ij}\rangle(t) = -i\int_{-\infty}^{\infty}dt'\theta(t-t')\left\langle[T_{ij}(t), \mathcal{J}_{kl}(t')]\frac{\partial\lambda_{\alpha\beta}(t')}{\partial t'}\right\rangle$$

$$= \int_{-\infty}^{\infty}dt'X_{ijkl}(t-t')\frac{\partial\lambda_{\alpha\beta}(t')}{\partial t'} \quad (17)$$

where

$$X_{ijkl}(t-t') = -i\theta(t-t')\langle[T_{ij}(t), \mathcal{J}_{kl}(t')]\rangle \quad (18)$$

is stress-strain correlation function and $\langle\cdots\rangle$ means average over disorder. The Fourier transformation of it is

$$X_{ijkl}(\Omega) = i\int_0^{\infty}dt\langle[T_{ij}(t), \mathcal{J}_{kl}(0)]\rangle e^{i\Omega^+ t} \quad (19)$$

where $\Omega^+ = \Omega + i0^+$. We can express Eq. (19) in an additional equivalent form as stress-stress form by using time-translation invariance and the relation

$$\int_0^{\infty}\mathcal{J}_{kl}(-t)e^{i\omega^+ t}dt = \int_{-\infty}^0 \mathcal{J}_{kl}(t)e^{-i\Omega^+ t}dt$$

$$= \frac{1}{-i\Omega^+}\left[\mathcal{J}_{kl}(0) + \int_0^{\infty}T_{kl}(-t)e^{i\Omega^+ t}dt\right] \quad (20)$$

based on

$$T_{ij} = \frac{i}{\hbar}[\mathcal{J}_{ij}, H] = -\frac{\partial\mathcal{J}_{ij}}{\partial t}. \quad (21)$$

Thus the response function can rewritten as

$$X_{ijkl}(\Omega) = \frac{1}{\Omega^+}\left\{\langle[T_{ij}(0), \mathcal{J}_{kl}(0)]\rangle\right.$$

$$\left. + \int_0^{\infty}dt\langle[T_{ij}(t), T_{kl}(0)]\rangle e^{i\Omega^+ t}\right\} \quad (22)$$

where the first term, which is called a contact term analogous to the diamagnetic conductivity, contributes to the bulk viscosity [31,43]. In this paper we focus on the shear and Hall viscosity, we then obtain the viscosity to be

$$\eta_{ijkl}(\Omega) = \frac{1}{\Omega^+ \mathcal{V}}\int_0^{\infty}dt\langle[T_{ij}(t), T_{kl}(0)]\rangle e^{i\Omega^+ t}, \quad (23)$$

which is called Kubo formula of viscosity. To calculate this retarded stress-stress correlation function, one can transform it into Matsubara function by analytical continuations $\Omega^+ \to i\Omega_n$ and $it \to \tau$,

$$\eta_{ijkl}(i\Omega_n) = \frac{1}{i}\frac{1}{i\Omega_n\mathcal{V}}\int_0^{\beta}d\tau\langle T_{\tau}T_{ij}(\tau)T_{kl}(0)\rangle e^{i\Omega_n\tau} \quad (24)$$

where the factor $\frac{1}{i}$ origins from $dt \to \frac{1}{i}d\tau$, and $\beta = \frac{1}{k_B T}$. For the disordered system, the integrand can be evaluated by the perturbation expansion as

$$\langle T_{\tau}T_{ij}(\tau)T_{kl}(0)\rangle = \frac{\langle T_{\tau}\psi^{\dagger}(\tau)T_{ij}\psi(\tau)\psi(0)^{\dagger}T_{kl}\psi(0)U_{\beta}\rangle_0}{\langle U_{\beta}\rangle_0} \quad (25)$$

where $\langle\cdots\rangle_0$ means the thermodynamic average over the eigenstates of unperturbed Hamiltonian and $U_\beta = T_\tau\{\exp[-\int_0^\beta d\tau' V(\tau')]\}$ is the time evolution operator in Matsubara formalism. By Wick' theorem and summations of Matsubara Green's functions with branch cuts, the Kubo formula Eq. (23) is written in terms of retarded (R) and advanced (A) Green's functions as

$$\eta_{ijkl}(\Omega) = -\frac{\hbar}{\Omega\mathcal{V}}\text{Tr}\int_{-\infty}^{\infty}\frac{d\omega}{2\pi}$$
$$\times\left[(f_{\omega+\Omega} - f_\omega)(T_{ij}G^R_{\omega+\Omega}T_{kl}G^A_\omega - T_{ij}G^A_{\omega+\Omega}T_{kl}G^A_\omega)\right.$$
$$\left. + f_\omega(T_{ij}G^R_{\omega+\Omega}T_{kl}G^R_\omega - T_{ij}G^A_{\omega+\Omega}T_{kl}G^A_\omega)\right] \quad (26)$$

where $f_\omega = \frac{1}{\exp[\beta(\omega - E)]+1}$ is the Fermi-Dirac distribution function. The detailed derivation of Eq. (26) is shown in the Supplemental Material Sec. 1 [44] (see, also, Refs. [45,46] and references therein).

D. Eigenbasis of the pure system and disorder-induced self-energy

In the absence of magnetic field, the eigenvalues and eigenstates of the pure graphene are

$$E_{ks} = s\hbar v_f k, \quad (27)$$

$$\Psi_{ks}(\mathbf{r}) = \langle\mathbf{r}|ks\rangle = \frac{e^{i\mathbf{k}\cdot\mathbf{r}}}{\sqrt{2A}}\begin{pmatrix}1\\se^{i\theta_k}\end{pmatrix}, \quad (28)$$

where $s = \pm$ denotes the chiral and A is the area of sample. The basis formed by Ψ_{ks} is called $(\mathbf{k}, s)$ basis. In this basis, the components of stress tensor T_{xy} and $T_{xx} - T_{yy}$, which will be used in the calculation of shear and Hall viscosity, are written as

$$T_{xy}(\mathbf{k}) = \frac{\hbar v_f k}{2}(\sigma_z\sin 2\theta_{\mathbf{k}} - \sigma_y\cos 2\theta_{\mathbf{k}}), \quad (29)$$

$$T_{xx}(\mathbf{k}) - T_{yy}(\mathbf{k}) = \hbar v_f k(\sigma_z\cos 2\theta_{\mathbf{k}} + \sigma_y\sin 2\theta_{\mathbf{k}}). \quad (30)$$

Then, we consider the graphene in the presence of a magnetic field perpendicular to the graphene, $\mathbf{B} = B\hat{z}$. The corresponding vector potential is given by $\mathbf{A} = Bx\hat{y}$ satisfying Landau gauge. The eigenenergy and eigenstates of the Hamiltonian in the magnetic field are

$$E_{n,k_y,s} = s\hbar\omega_c\sqrt{n}; \quad s = \pm 1; \quad n = 0, 1, 2, \cdots \quad (31)$$

and

$$\Psi_{n,k_y,s}(x, y) = \frac{e^{ik_y y}}{\sqrt{L_y}}\begin{cases}(0, \quad \phi_{0,k_y})^T; & n = 0\\\frac{1}{\sqrt{2}}(-is\phi_{n-1,k_y}, \quad \phi_{n,k_y})^T; & n \neq 0\end{cases} \quad (32)$$

with

$$\phi_{n,k_y}(x) = \sqrt{\frac{1}{2^n n!\sqrt{\pi}l_B}}e^{-\left(\frac{x}{l_B}+l_Bk_y\right)^2/2}H_n\left(\frac{x}{l_B}+l_Bk_y\right) \quad (33)$$

where $l_B = \sqrt{\hbar/eB}$ is magnetic length, $\omega_c = \sqrt{2}v_f/l_B$ is cyclotron frequency. The basis formed by $\Psi_{n,k_y,s}$ is called (n, k_y, s) basis. In this basis, the components of stress tensor T_{xy} and $T_{xx} - T_{yy}$ are written as

$$\langle n, k_y, s|T_{xy}|n', k_y', s'\rangle$$
$$= \delta_{k_y,k_y'}\begin{cases}0; & n = n' = 0\\-is'\frac{\hbar\omega_c}{2\sqrt{2}}\delta_{0,n'-2}; & n = 0, n' \neq 0\\is\frac{\hbar\omega_c}{2\sqrt{2}}\delta_{0,n-2}; & n \neq 0, n' = 0\\\frac{\hbar\omega_c}{4}(is\sqrt{n-1}\delta_{n,n'+2} - is'\sqrt{n+1}\delta_{n,n'-2}); & n, n' \neq 0\end{cases} \quad (34)$$

$$\langle n, k_y, s|T_{xx} - T_{yy}|n', k_y', s'\rangle$$
$$= \delta_{k_y,k_y'}\begin{cases}0; & n = n' = 0\\-s'\frac{\hbar\omega_c}{\sqrt{2}}\delta_{0,n'-2}; & n = 0, n' \neq 0\\-s\frac{\hbar\omega_c}{\sqrt{2}}\delta_{n-2,0}; & n \neq 0, n' = 0\\-(s\sqrt{n-1}\delta_{n',n-2} + s'\sqrt{n+1}\delta_{n',n+2}); & n, n' \neq 0\end{cases} \quad (35)$$

which can be easily derived by the second quantization shown in the Supplemental Material Sec. 2 [44].

The disorder $V(\mathbf{r})$ we considered is a short-range random potential having form in the $\mathbf{r}$ space as

$$V(\mathbf{r}) = \sum_i^{N_i} V_i\delta(\mathbf{r} - \mathbf{r}_i) \quad (36)$$

with random strength distribution satisfying $\overline{V(\mathbf{r})} = 0$ and $\overline{V(\mathbf{r})V(\mathbf{r}')} = n_i V_0^2\delta(\mathbf{r} - \mathbf{r}')$, where $\overline{\cdots}$ stands for averaging over disorder realizations, V_0^2 is the variance of impurity strength, and $n_i = N_i/\mathcal{V}$ is the concentration of impurity. In the following, we show the analytic expression of self-energy function based on self-consistent Born approximation

(SCBA) (details in the Supplemental Material Sec. 3 [44]), and express the density of state in term of self-energy. In this paper, we assume the SCBA is applicable for Dirac electrons. To explicitly justify the SCBA is out of the scope of this paper. Additionally, we stress that the main results shown in this paper do not rely on the SCBA. Our starting point is a finite self-energy function induced by impurity scattering [47–49].

a. In the absence of magnetic field $B = 0$.

At first, we evaluate the self-energy with SCBA in the absence of magnetic field

$$\Sigma(E) = \frac{2(\hbar v_f)^2}{A}\int dk k\frac{E - \Sigma}{(E - \Sigma)^2 - (\hbar v_f k)^2} \quad (37)$$

where $A = \frac{4\pi(\hbar v_f)^2}{n_i V_0^2}$ is the dimensionless parameter characterizing the scattering strength. The solution of the above self-consistent equation in weak-disorder limit is given by [50]

$$\text{Im}\Sigma(E) = -E_c e^{-A/2} - \frac{\pi}{A}|E| \qquad (38)$$

where $E_c \approx 7.2$ eV is the energy cutoff. The density of states in terms of self-energy is given by

$$\rho(E) = -\frac{2A}{\pi^2(\hbar v_f)^2}\text{Im}\Sigma(E). \qquad (39)$$

b. In the presence of magnetic field $B \neq 0$.

In the presence of magnetic field, we write the SCBA equation of self-energy in Landau quantized (n, k_y, s) basis,

$$\Sigma(E) = \overline{\langle n, k_y, s|VG(E)V|n, k_y, s\rangle} = \frac{(\hbar\omega_c)^2}{2A}\sum_{ns} G_{ns}(E) \qquad (40)$$

where $G_{ns}(E) = (E - s\sqrt{n}\hbar\omega_c - \Sigma)^{-1}$ is the Green's function in the (n, k_y, s) basis. $\omega_c = \sqrt{2}v_f/l_B$ is cyclotron frequency, $l_B = \sqrt{\hbar/eB}$ is magnetic length. Similar to the case of 2DEG, we consider the graphene in the presence of magnetic field in two classes: "well separated" region, where the Landau levels are well separated with each other, and 'overlapped' region, where the Landau subbands broaden and overlap with each other due to the disorder scattering. While the criterion distinguishing these two regions in 2DEG is the product of the cyclotron frequency, which is determined by the magnetic field, and the relaxation time, which is determined by the disorder strength, in graphene, due to the uneven distribution of Landau levels, it should also consider the location of the Fermi level. Thus, we introduce an effective cyclotron frequency $\tilde{\omega}_c = \frac{\hbar\omega_c^2}{2|E|}$, which can tend to the expression of cyclotron frequency in 2DEG, i.e., $\tilde{\omega}_c = \frac{eB}{m}$, by using effective mass $m = \frac{2|E|}{v_f^2}$. Then the "well separated" region and "overlapped" region are divided by $\tilde{\Omega}_c\tau \gg 1$ and $\tilde{\Omega}_c\tau \lesssim 1$.

In the region of well separated Landau levels, we get

$$\text{Im}\Sigma(E) = -\hbar\omega_c\sqrt{\frac{1}{2A} - \varepsilon^2} \qquad (41)$$

where the Fermi energy E is assumed locating close to the Landau level E_{NS} and the distance is characterized by the $\varepsilon = (E - E_{NS})/2\hbar\omega_c$.

In the region of overlapped Landau levels,

$$\text{Im}\Sigma(E) = -E_c e^{-A/2} - \frac{(\hbar\omega_c)^2}{2E_c e^{-A/2}} - \frac{\pi}{A}|E|\left[1 + 2\delta\cos\frac{\pi E}{\hbar\tilde{\omega}_c}\right] \qquad (42)$$

where $\delta = e^{-\frac{4\pi^2 E^2}{A(\hbar\omega_c)^2}}$.

In this condition, the density of states is expressed as

$$\rho(E) = -\frac{2}{\pi^2 l_B^2}\frac{2A}{(\hbar\omega_c)^2}\text{Im}\Sigma(E). \qquad (43)$$

III. STATIC VISCOSITY

A. Static shear viscosity η_S

We start from evaluating the static shear viscosity η_S in graphene at the zero temperature: It can be obtained by the real part of Kubo formula Eq. (26) with the stress tensor components chosen as $T_{ij} = T_{kl} = T_{xy}$,

$$\eta_s(E) = \text{Re}\left[\eta_s^{RA}(E) - \eta_s^{RR}(E)\right] \qquad (44)$$

with

$$\eta_s^{LM}(E) = 4\frac{\hbar}{2\pi\mathcal{V}}\text{Tr}\left[G^L(E)T_{xy}G^M(E)T_{xy}\right] \qquad (45)$$

where $L, M = R, A$ denotes the retarded and advanced Green's function and the factor 4 denotes the degeneracy of spin and valley. In the Boltzmann transport theory, the contribution from the retarded-retarded (RR) channel is usually discarded. In the studies of quantum conductivity of graphene, however, this term becomes as much relevant as the RA one in proximity to Dirac point [51]. In this paper for viscosity, we also find η_s^{RR} cannot be neglected in vicinity of Dirac point.

In the following, we will calculate and analyze the shear viscosity in the two cases: (1) in the absence of magnetic field, $\boldsymbol{B} = 0$; (2) in the presence of a magnetic field perpendicular to the xy plane, $\boldsymbol{B} = B\hat{z}$. The vertex corrections of the Kubo formula for viscosity in both cases $\boldsymbol{B} = 0$ and $\boldsymbol{B} = B\hat{z}$ are proved to be zero due to short-range disorder scattering in the Supplemental Material Sec. 4 [44]. A plausible explanation is given by analogizing the vertex correction in Kubo formula to the transport relaxation time correction in Boltzmann transport theory, which is a scheme to distinguish the contributions of forward scattering and back scattering. The Kubo formula for viscosity is in nature a stress-stress correlation function and the stress is an product of velocity and momentum. Therefore, the effect of short-range disorder consisting of uniformly distributed plane waves in the momentum space on viscosity isotropic due to a nontrivial compensation between the velocity direction and momentum direction.

1. $B = 0$

In the absence of magnetic field, the η_s^{LM} in Eq. (45) can be expanded in the $(\boldsymbol{k}, s)$ basis and given by

$$\eta_s^{LM}(E) = \frac{\hbar^3 v_f^2}{8\pi^2}\int dk k^3 (g_+^L + g_-^L)(g_+^M + g_-^M) \qquad (46)$$

where $g_\pm^{R/A}(E) = (E \mp \hbar v_f k - \Sigma^{R/A})^{-1}$ is the full Green's function in the $(\boldsymbol{k}, s)$ basis with self-energy $\Sigma^{R/A}$ approximately obtained from the SCBA equation (37). The detail of analytic derivation of η_s^{LM} is performed in the Supplemental Material Sec. 5 [44]. η_s^{RA} finally arrives at $\eta_s^{RA}(E) = \frac{1}{8}E^2\rho\tau + \frac{\hbar^2}{32\tau}\rho$, where $\tau = \frac{\hbar}{2|\text{Im}\Sigma(E)|}$ is the quasiparticle relaxation time. The real part of η_s^{RR} approaches to $\text{Re}\eta_s^{RR}(E) = -\frac{\hbar^2}{16\tau}\rho$, which
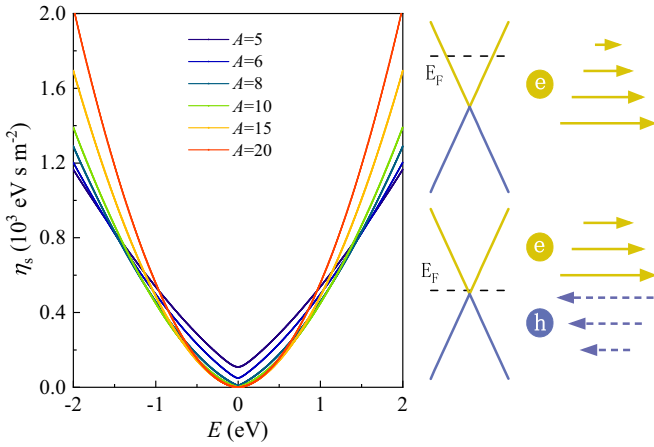
FIG. 1. (Left) Numerical result for the shear viscosity η_s as a function of Fermi energy in the absence of magnetic field. $A = \frac{4\pi(\hbar v_f)^2}{n_i V_0^2}$ is a dimensionless parameter characterizing the scattering strength (see main text). (Right) Cartoon picture for hydrodynamic flow for doped and undoped graphene.

is as much relevant as η_s^{RA} in the limit $E \to 0$. The total real part of shear viscosity, therefore, is obtained as

$$\eta_s(E) = \frac{1}{8}E^2\rho\tau + \frac{3}{32}\frac{\hbar^2\rho}{\tau}. \quad (47)$$

If we plug the expressions of self-energy Eq. (38) and density of states Eq. (39) into the above result, it can be rewritten as

$$\eta_s(E) = \frac{\hbar}{8\pi^2(\hbar v_f)^2}\left[AE^2 + \frac{3}{A}(\pi|E| + E_c A e^{-A/2})^2\right]. \quad (48)$$

The first term in Eq. (47) and Eq. (48) is in accordance with that in 2DEG, and can also be written as $\frac{1}{4}m\bar{n}v_f l$, where $m = |E|/v_f^2$ is the effective mass, $\bar{n} = \int \rho dE \approx \frac{1}{2}\rho|E|$ is the average charge density, and $l = v_f\tau$ is mean free path. The second term, which does not exist in 2DEG, is inversely proportional to the quasiparticle relaxation time and implies the viscosity will be enhanced by disorder potential near the Dirac point. This is inconsistent with ordinary metals and classical fluids, where impurities can pack to eliminate any sign of collective behavior of particles. Similar to the minimal conductivity of graphene due to impurity assisted resonant tunneling through the electron-hole coherence and retarded-retarded (RR) channel [51]; this anomalous term in static shear viscosity also mainly comes from the electron-hole coherence and RR term. However, in distinction to the charge current, the momentum current also contains single-particle contributions. Thus, the disorder-assisted transport is significantly larger in viscosity compared to conductivity.

In order to clearly see the effect of the anomalous term in η_s, we also performed the numerical calculation of the Eq. (46) and the SCBA equation (37) of the self-energy function. The results for several different disorder strengths are illustrated in Fig. 1. The relationship between η_s and

disorder scattering can be divided into two regions with opposite behaviors. In the high-energy region that we call the "normal region", η_s decays rapidly with the increasing of disorder scattering. This is consistent with the 2DEG and classical fluids. In the low-energy region roughly $[-1.1$ eV, 1.1 eV], which we call "anomalous region", η_s has a peculiar enhancement induced by disorder. It well agrees with the analytic prediction in Eq. (47). Furthermore, the range of this "anomalous region" is quite large, not just the interval extremely close to the Dirac point, which is consistent with the hydrodynamic transport region detected in experiments [2–4]. Intuitively, the different observation in doped and undoped graphene can be understood by the pictures as illustrated in Fig. 1: In the updoped case in the vicinity of Dirac point, electrons flow in the direction opposite to the holes, and frequent electron-hole collisions leads to enhancement of hydrodynamic behavior. While in the doped case with a large Fermi surface, only one type of carriers contributes so the hydrodynamic behavior should be similar to that of normal Fermi liquid. Moreover, for the clean system, both the analytic and numerical results indicate that η_s vanishes at the Dirac point, which essentially originates from the zero density of states in this condition, since the electron-electron interaction is neglected in this paper.

2. $B \neq 0$

Under a magnetic field perpendicular to the graphene, we expand the Kubo formula Eq. (44) into the (n, k_y, s) basis (see the Supplemental Material Sec. 2 [44]), and get

$$\eta_s^{LM}(E) = \frac{(\hbar\omega_c)^2}{4\pi^2 l_B^2}\sum_n (n+1)\text{Re}\left(g_n^L g_{n+2}^M + g_n^M g_{n+2}^L\right) \quad (49)$$

where $g_n^{R/A} = \frac{1}{2}(G_{n,+}^{R/A} + G_{n,-}^{R/A}) = \frac{E - \Sigma^{R/A}}{(E - \Sigma^{R/A})^2 - n(\hbar\omega_c)^2}$. The derivation of the analytic expression of η_s for $B \neq 0$ is separated into two classes, and are displayed in the Supplemental Material Sec. 6 [44]. When the Landau levels are well separated, i.e., $\tilde{\omega}_c\tau \gg 1$, we get

$$\eta_s(E) = (N^2 + \delta_{N,0})\frac{\hbar}{2\pi^2 l_B^2}(1 - 2A\varepsilon^2) \quad (50)$$

where $\varepsilon = (E - E_{NS})/2\hbar\omega_c$ characterizes the distance between the Fermi energy and the center of nearest Landau level. The predicted values of static shear viscosity at the center of Landau levels are quantized as $\eta_s = (N^2 + \delta_{N,0})\frac{\hbar}{2\pi^2 l_B^2}$. When the Landau levels are overlapped ($\tilde{\omega}_c\tau \lesssim 1$), η_s is approximately given by

$$\eta_s = \frac{1}{8}\frac{E^2\rho\tau}{1 + 4\tilde{\omega}_c^2\tau^2} + \frac{\hbar^2}{32\tau}\rho\frac{3 + 16\tilde{\omega}_c^2\tau^2}{1 + 4\tilde{\omega}_c^2\tau^2} \quad (51)$$

The first term in this result is consistent with the result for 2DEG [26], except for the cyclotron frequency $\tilde{\omega}_c$, which depends on both magnetic field and Fermi energy in graphene but only depends on magnetic field in 2DEG. Since the well separated and overlapped regions are determined by the value of $\tilde{\omega}_c\tau$, the relation $\tilde{\omega}_c \propto \frac{1}{|E|}$ means that the separated

region in graphene is close to the Dirac point. The second term, which can reduce to the anomalous term in Eq. (47) when $\tilde{\omega}_c \to 0$, is positively related to both disorder scattering and magnetic field strength according to the self-energy equation (42). After plugging the self-energy function (42) and density of states (43) into Eq. (51), the static shear viscosity can be further evaluated by separated the states into $|E|/\hbar\omega_c > 1$ and $|E|/\hbar\omega_c \lesssim 1$. For the states $|E|/\hbar\omega_c > 1$, the static shear viscosity is obtained as

$$\eta_s(E) = \frac{\hbar}{4\pi^2 l_B^2} \frac{AE^2}{(\hbar\omega_c)^2(1+4\alpha^2)} \left[1 + \frac{4\alpha^2\delta}{1+4\alpha^2}\cos\frac{\pi E}{\hbar\tilde{\omega}_c}\right] \tag{52}$$

where $\alpha = \frac{A}{\pi}\frac{\hbar\tilde{\omega}_c}{E}$ and $\delta = e^{-\frac{4\pi^2 E^2}{A(\hbar\omega_c)^2}}$. The second term in the above expression exhibits Shubnikov-de Haas-type oscillations, but the contribution of this term will be suppressed as E increases since the parameters α and δ both decrease with E.

For the states $|E|/\hbar\omega_c \lesssim 1$, which are in the vicinity of Dirac point, the static shear viscosity can be approximately given by

$$\eta_s(E) = \frac{3A}{8\pi^2\hbar^2 v_f^2}\left[E_c e^{-A/2} + \frac{\hbar v_f^2}{E_c e^{-A/2}} eB\right]^2 \quad, \tag{53}$$

which is positively related to the strength of magnetic field.

In Fig. 2 we show the numerical results of η_s in the presence of magnetic field, which are obtained by numerically solving Kubo formula (49) and self-energy equation (40). As shown in Fig. 2(a), the curves of $\eta_s(E)$ with different disorder strength change from separated peaks to Shubnikov-de Haas-type oscillations and then to smooth, which is consistent with the prediction of analytic solutions. From the inset in Fig. 2(a), one can also find an anomalous disorder-induced shear viscosity enhancement behavior in the low-energy region, similar to the case in the absence of a magnetic field. Furthermore, for the states near the Dirac point, the shear viscosity can also be enhanced by magnitude of the applied magnetic field B as shown in Fig. 2(b). This behavior is contract to the 2DEG, where the static shear viscosity decays with B as a function, $\eta_s \propto \frac{B_0^2}{B_0^2+B^2}$ [28].

B. Static Hall viscosity η_H

The Hall viscosity is an example of "anomalous transport coefficients", which only exists in the time-reversal symmetry broken systems. It can also be represented by the strain-induced Berry curvature of wave function and therefore exhibit the striking phenomenon of topology when the Fermi level falls in a spectral gap [29,32,52].

Here, we focus on the static Hall viscosity η_H in the presence of magnetic field perpendicular to the graphene plane. It can be calculated by the real part of Kubo formula Eq. (26) with $T_{ij} = T_{xy}$, $T_{kl} = \frac{1}{2}(T_{xx} - T_{yy})$,

$$\eta_H(E) = \text{Re}\left[\eta_H^{I,RA}(E) - \eta_H^{I,RR}(E) + \eta_H^{II}(E)\right] \tag{54}$$

where

$$\eta_H^{I,LM}(E) = 4\frac{\hbar}{4\pi\mathcal{V}}\text{Tr}[G^L(E)(T_{xy} - T_{yy})G^M(E)T_{xy}], \tag{55}$$
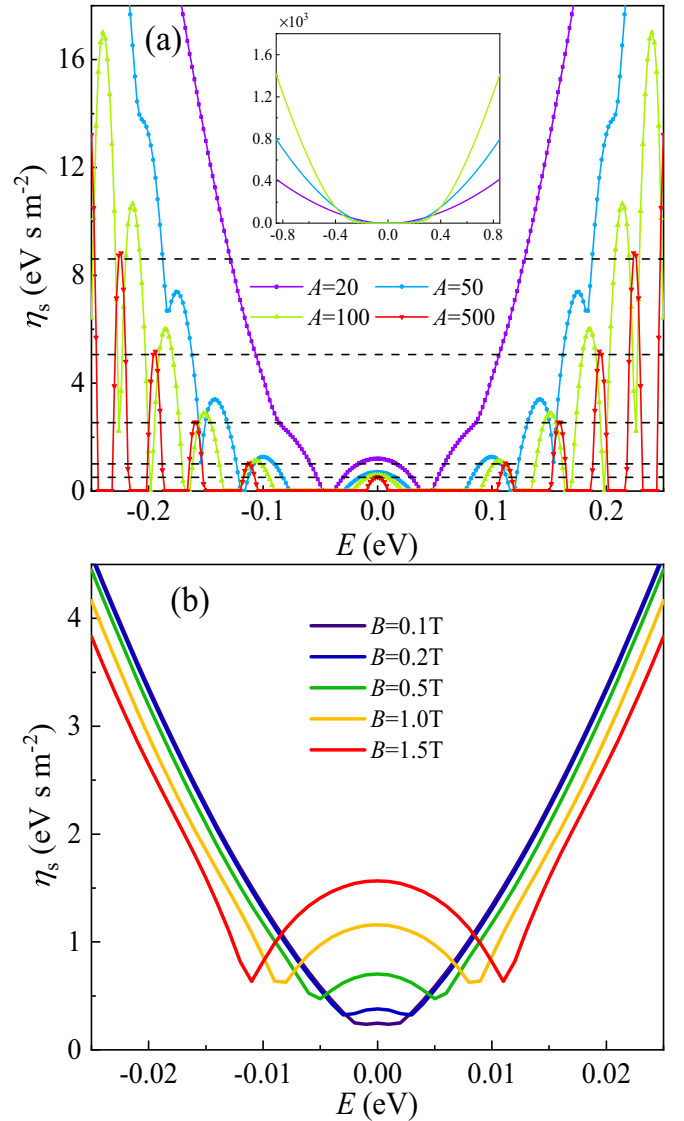
FIG. 2. (a) Static η_s as E for fixed magnetic field strength $B = 10$ T and different disorder scattering $A = \frac{4\pi(\hbar v_f)^2}{n_i V_0^2} = 20, 50, 100, 500$. Dashed lines in top pane denote the predicted values of static shear viscosity of each Landau level in the absence of disorder, $\eta_s = (N^2 + \delta_{N,0})\frac{\hbar}{2\pi^2 l_B^2}$. The inset is the same plot with a larger energy scope. (b) Static η_s vs E for fixed $A = 15$ and $B = 0.1$ T, 0.2 T, 0.5 T, 1 T, 1.5 T.

$$\eta_H^{II}(E) = 4\frac{\hbar}{4\pi\mathcal{V}}\int d\omega f_\omega \text{Tr}\left[G^R(\omega)(T_{xy} - T_{yy})\frac{dG^R(\omega)}{d\omega}T_{xy}\right.$$
$$\left. - \frac{dG^R(\omega)}{d\omega}(T_{xy} - T_{yy})G^R(\omega)T_{xy}\right], \tag{56}$$

which is analogous to the Kubo-Streda formula of the Hall conductivity. Compared with η_s, the Kubo formula of η_H has an extra term η^{II}. η^{II} is strikingly different from terms $\eta^{I,LM}$ in that it contains contributions from the entire Fermi sea, while $\eta^{I,LM}$ only from electron states at the Fermi surface. After plugging the expressions of stress tensor $T_{xx} - T_{yy}$ and T_{xy}, the

$\eta_H^{I,LM}$ and η_H^{II} are reduced as

$$\eta_H^{LM} = \frac{i\hbar^3 \omega_c^2}{16\pi^2 l_B^2} \sum_{n,s,s'} (n+1)\left[G_{n+2,s}^L(E)G_{n,s'}^M(E) \right.$$
$$\left. - G_{n,s}^L(E)G_{n+2,s'}^M(E)\right], \tag{57}$$

$$\eta_H^{II} = \frac{i\hbar^3 \omega_c^2}{8\pi^2 l_B^2} \int f_\omega d\omega \sum_{nss'} (n+1)$$
$$\times \left[G_{n+2,s}^R(\omega)\frac{dG_{ns'}^R(\omega)}{d\omega} - G_{ns'}^R(\omega)\frac{dG_{n+2,s}^R(\omega)}{d\omega}\right]. \tag{58}$$

Obviously, $\eta^{I,RR}$ vanishes, so the contribution of Fermi surface states is only reflected in $\eta_H^{I,RA}$, which is calculated in the Supplemental Material Sec. 7 [44]

$$\eta_H^{I,RA}(E) = \frac{1}{4}\frac{\rho\tilde{\omega}_c\tau^2 E^2}{1+4\tilde{\omega}_c^2\tau^2}. \tag{59}$$

The real part of η_H^{II} is

$$\text{Re}\eta_H^{II}(E) = \frac{\hbar}{8\pi^2 l_B^2}\left\{E\sum_{ns}(2n+\delta_{n,0})\text{Im}G_{ns}^R(E)\right.$$
$$- 2\int d\omega f(\omega)\sum_{ns}(n+1)^2$$
$$\left.\times \left[\text{Im}G_{ns}^R(\omega) - \text{Im}G_{n+2,s}^R(\omega)\right]\right\}. \tag{60}$$

Since the broaden of the Landau level will strikingly affect the value of $\text{Im}G_{ns}^R(\omega) - \text{Im}G_{n+2,s}^R(\omega)$, the real part of η_H^{II} is evaluated in the separated and overlapped region, respectively. In the separated region ($\tilde{\omega}_c\tau \gg 1$),

$$\text{Re}\eta_H^{II}(E) \approx -\frac{E^2\rho}{16\tilde{\omega}_c} + \text{sgn}(E)\frac{\hbar}{4\pi l_B^2}(2N^2+2N+1). \tag{61}$$

In the overlapped region ($\tilde{\omega}_c\tau \ll 1$),

$$\text{Re}\eta_H^{II}(E) = -\frac{\hbar E^3}{2(\hbar\omega)^2}\rho(E) + \frac{2\hbar}{(\hbar\omega_c)^2}\int_0^E d\omega\omega^2\rho(\omega) \approx 0. \tag{62}$$

Thus, the analytic expression of the total static Hall viscosity η_H is

$$\eta_H(E) = \begin{cases} \frac{\text{sgn}(E)(2N^2+2N+1)\hbar}{4\pi l_B^2} - \frac{1}{16\tilde{\omega}_c}\frac{\rho E^2}{1+4\tilde{\omega}_c^2\tau^2}; & \tilde{\omega}_c\tau \gg 1 \\ \frac{1}{4}\frac{\rho\tilde{\omega}_c\tau^2 E^2}{1+4\tilde{\omega}_c^2\tau^2}; & \tilde{\omega}_c\tau \ll 1 \end{cases}. \tag{63}$$

From this result, we find the behavior of static Hall viscosity is somewhat similar to the Hall conductivity. It is also quantized in the Landau level gaps where the density of states vanishes, and has opposite signs for the electron states and hole states. At the same time, η_H is not integral quantized
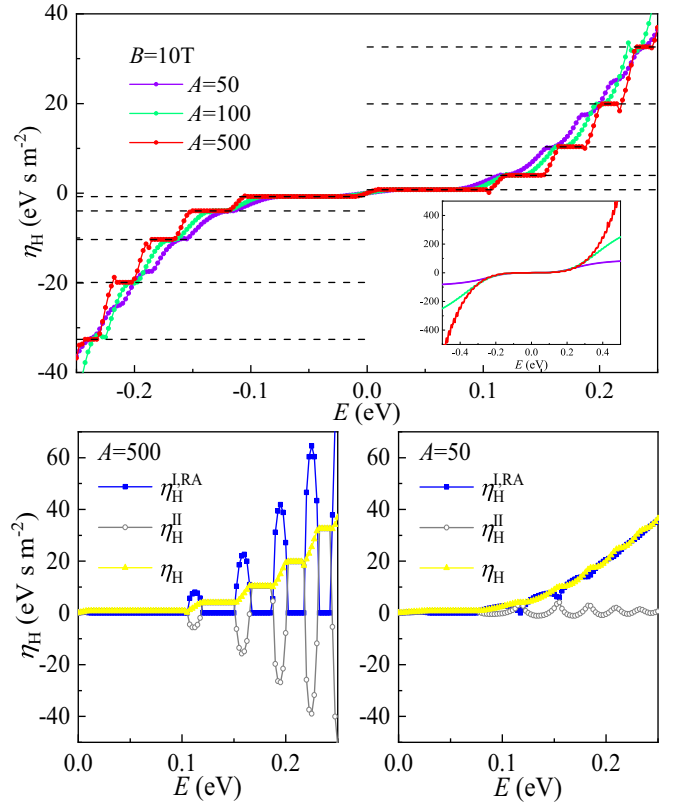
FIG. 3. (Top) dc Hall viscosity η_H as a function of Fermi energy E for fixed magnetic field strength $B = 10$ T and different disorder scattering $A = \frac{4\pi(\hbar v_f)^2}{n_i V_0^2} = 50, 100, 500$. Dashed lines denote the predicted values of Hall viscosity of each Landau level in the absence of disorder, $\eta_H = \frac{\text{sgn}(E)(2N^2+2N+1)\hbar}{4\pi l_B^2}$. (Bottom) Different contributions of η_H (see main text).

but has an additional $1/4$, which is analogy to the additional $1/2$ in Hall conductivity of graphene, both of which are the hallmark of the chiral nature of graphene [53]. Besides, we find that the quantized value is mainly contributed from the Fermi sea states, i.e., η_H^{II}. With the overlap of the Landau levels, the contribution from Fermi sea fades and the contribution from Fermi surface states increases. Therefore, when the Landau level gaps are smoothed by the decrease of $\tilde{\omega}_c\tau$, the quantization behavior of η_H disappears.

In Fig. 3, we show the numerical results of η_H for a fixed magnetic field strength $B = 10$ T and different disorder scattering strengths: $A = 50, 100,$ and 500 (top pane), and compare the different contributions from $\eta_H^{I,RA}$ and η_H^{II} at $A = 50$ and 500 (bottom pane). For the extremely small scattering $A = 500$ close to pure graphene, it can be clearly seen that η_H has a step structure. The height of the step in the Landau level gap is well consistent with the analytically prediction, $\eta_H = \frac{\text{sgn}(E)(2N^2+2N+1)\hbar}{4\pi l_B^2}$. When the disorder scattering is strengthened, the plateau of the step structure shrinks due to the broaden of Landau levels, and the center of plateau slightly moves to zero energy due to the shift of Landau levels. Furthermore, just as predicted in Eq. (62), the contribution from Fermi sea η^{II} is fading away with the overlap of Landau levels.

IV. DYNAMIC VISCOSITY

A. Dynamic shear viscosity $\eta_s(\Omega)$

Now, we turn to the dynamic shear viscosity $\eta_S(\Omega)$ in graphene. In this case, the Kubo formula of η_s is simplified as $\eta_s(E) = \text{Re}[\eta_s^{RA}(E) - \eta_s^{RR}(E)]$ with

$$\eta_s^{LM}(\Omega) = -4\frac{\hbar}{2\pi\mathcal{V}}\int_{-\infty}^{\infty}d\omega\frac{f_{\omega+\Omega}-f_\omega}{\Omega}\text{Tr}[G_{\omega+\Omega}^L T_{xy}G_\omega^M T_{xy}]. \quad (64)$$

Similar to the static shear viscosity, we separate the calculation of dynamic shear viscosity into two conditions: $\boldsymbol{B} = 0$ and $\boldsymbol{B} = B\hat{z}$.

1. $\boldsymbol{B} = 0$

In the absence of magnetic field, we rewrite $\eta_s^{LM}(\Omega)$ in the $(\boldsymbol{k}, s)$ basis as

$$\eta_s^{LM}(\Omega) = -\frac{\hbar^3 v_f^2}{8\pi^2}\int_{-\infty}^{\infty}d\omega\frac{f_{\omega+\Omega}-f_\omega}{\Omega}$$
$$\times \int dk k^3[g_+^L(\omega+\Omega)+g_-^L(\omega+\Omega)]$$
$$\times [g_+^M(\omega)+g_-^M(\omega)]. \quad (65)$$

When $\hbar\Omega \to 0$, the dynamic shear viscosity $\eta_s(\Omega)$ reverts to the static shear viscosity described in Sec. III A. At zero temperature, f_ω tends to be a step function. According to the term $f_{\omega+\Omega} - f_\omega$ in Eq. (65), the states that contribute to $\eta_s(\Omega)$ need locate on the two sides of Fermi surface, which means that the frequencies $\omega + \Omega$ and ω in the integrand should satisfy $\omega < E < \omega + \Omega$ for $\Omega > 0$, and $\omega - \Omega < E < \omega$ for $\Omega < 0$. In this section, we will evaluate the $\eta_s(\Omega)$ under two other constraints at zero temperature: (1) $E \approx 0 \ll \Omega$ and (2) $0 < \Omega \ll E$. Due to the electron-hole symmetry in graphene, the condition for negative Ω is symmetric to the case for positive Ω and is therefore ignored. Under the first condition that implies $\omega < 0 < \omega + \Omega$ in Eq. (65), the contribution from electron-hole (e-h) coherence plays a dominant role. In contrast, under the second condition, which implies $0 < \omega \lesssim \omega + \Omega$, the electron-electron (e-e) coherent contribution due to collisions of thermally excited carriers is dominant. The analytic derivation of $\eta_s(\Omega)$ in these two conditions is displayed in the Supplemental Material Sec. 8 [44].

In the e-h dominant region $E \ll \Omega$, the $\eta_s(\Omega)$ is given by

$$\eta_s(\Omega) = \frac{\Omega^2}{16\hbar v_f^2}\left(\frac{1}{2} + \frac{16}{15}\frac{1}{A}\right), \quad (66)$$

In the e-e dominant region $0 < \Omega \ll E$, the $\eta_s(\Omega)$ arrives at

$$\eta_s(\Omega) = \frac{E^2}{2\pi^2\hbar v_f^2}\left(\frac{\pi^2}{A} + \frac{AE^2}{\frac{A^2}{\pi^2}\Omega^2 + 4E^2}\right). \quad (67)$$

We compare and analyze these two results for dynamic shear viscosity in the e-h dominant and e-e dominant regions from both frequency-dependent and disorder effects perspectives. We find that the dynamic shear viscosity η_s is positively correlated with frequency Ω in the e-h dominant region, but negatively correlated with frequency Ω in the e-e dominant region. The dependence of $\eta_s(\Omega)$ on disorder scattering is
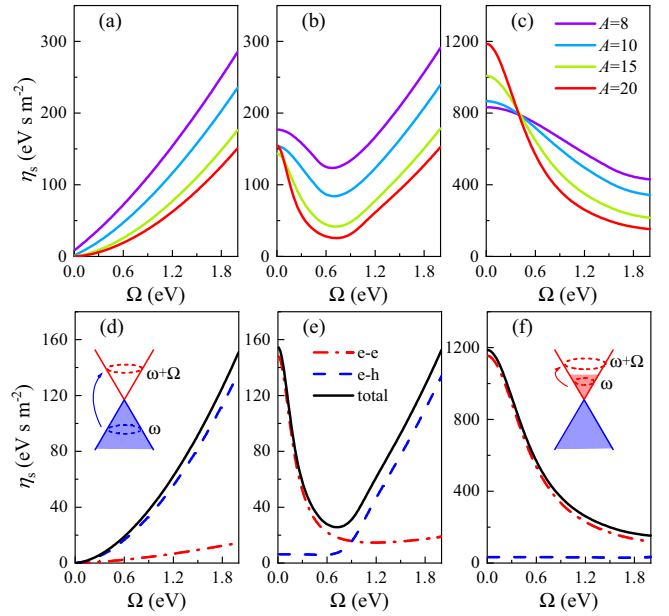
FIG. 4. [(a)–(c)] Numerical results of as shear viscosity η_s vs frequency $\hbar\Omega$ in the disordered graphene at zero temperature with Fermi energy: (a) $E = 0$ eV; (b) $E = 0.5$ eV; and (c) $E = 1.5$ eV. [(d),(e)] Comparison of the contributions of electron-electron (e-e) coherence and electron-hole (e-h) coherence for disorder scattering $A = 20$ and Fermi energy corresponding to [(a)–(c)]. The insets in (d) and (f) are the sketches of e-e coherence and e-h coherence.

more complicated. In the e-h dominant region, η_s is monotonically increasing with the disorder scattering. When the e-h coherence is dominant, however, η_s also relies on the Fermi energy. As disorder scattering increases, η_s declines at $4E^2 \gg \frac{A^2}{\pi^2}\Omega^2$ and strengthens at $4E^2 \ll \frac{A^2}{\pi^2}\Omega^2$. This opposite behavior of dynamic η_s versus disorder scattering over different Fermi energy region is reminiscent of the static shear viscosity shown in Fig. 1, where one finds similar behaviors in two different regions: "normal region" ($|E| > 1.1$ eV) and "anomalous region" ($|E| \lesssim 1.1$ eV).

To clearly show the above properties of dynamic shear viscosity, we also illustrate the numerical results of η_s versus Ω in the disordered graphene at zero temperature in Figs. 4(a)–4(c), where the Fermi energies are set to $E = 0$ eV, 0.5 eV, and 1.5 eV. In the results of $E = 0.0$ eV, which belongs to e-h dominant region, η_s increases superlinearly with Ω and decreases with A, both behaviors are well agree with the analytic prediction Eq. (66). In the case of $E = 1.5$ eV and low frequency, which belongs to e-e dominant region, η_s drops sharply with Ω, and the $\eta_s(\Omega)$ curves of different disorder strengths have a cross. These behaviors also meet expectation of Eq. (67). In the case of $E = 0.5$ eV, the transition between the e-h dominant region and e-e dominant region can be seen. The different transport mechanisms for these Fermi energies are also demonstrated by comparing of the contributions of electron-electron coherence and electron-hole coherence in Figs. 4(d) and 4(e).

Another remarkable piece of information we gain from the numerical results is a link between dynamic and static shear viscosities. We introduced "normal region" ($|E| > 1.1$ eV)
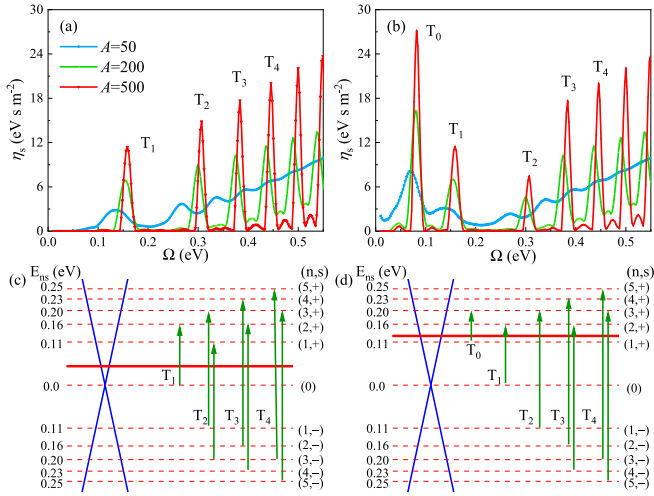
FIG. 5. [(a),(b)] The numerical results of η_s vs Ω for the magnetic field $B = 10$ T and Fermi energy: (a) $E = 0.05$ eV and (b) $E = 0.13$ eV. [(c),(d)] The schematic representation of the transitions correspond to the peaks T_i in [(a),(b)].

and "anomalous region" ($|E| \lesssim 1.1$ eV) when analyzing the static shear viscosity. In the case of $E = 1.5$ eV, the increase of Ω can let available ω cross the "normal region" into "anomalous region". The critical frequency is $\hbar\Omega \approx 0.4$ eV, which quite matches the cross point shown in Fig. 4(c).

2. $B \neq 0$

In the presence of magnetic field $\boldsymbol{B} = B\hat{z}$, the total dynamic $\eta_s(\Omega) = \text{Re}[\eta_s^{RA}(\Omega) - \eta_s^{RR}(\Omega)]$ can be written as

$$
\eta_s(\Omega) = -\frac{\hbar^3 \omega_c^2}{8\pi^2 l_B^2} \int_{-\infty}^{\infty} d\omega \frac{f_{\omega+\Omega} - f_\omega}{\Omega} \sum_{n,s,s'} (n+1)
$$
$$
\times \left[\text{Im}G_{ns}^R(\omega + \Omega)\text{Im}G_{n+2,s'}^R(\omega) + (\omega + \Omega \leftrightarrow \omega) \right].
$$
$$(68)$$

At the well separated Landau levels region and zero temperature, it is evaluated as

$$
\eta_s(\Omega) = \frac{\hbar^3 \omega_c^2}{8 l_B^2} \sum_{n,s,s'} \frac{n+1}{\Omega}
$$
$$
\times \left[(f_{E_{ns}} - f_{E_{n+2,s'}})\delta(\Omega + E_{n+2,s'} - E_{ns}) \right.
$$
$$
\left. + (E_{ns} \leftrightarrow E_{n+2,s'}) \right].
$$
$$(69)$$

From Eq. (69), one can easily find that in this case the dynamic shear viscosity is determined by the state transitions between Landau levels, $E_{ns} \leftrightarrow E_{ms'}$, where the level indices satisfy $|m - n| = 2$ and there is no restriction on s and s'. Similar selection rule exists in the calculation of magneto-optical conductivity in graphene, but in which level index of the allowed transitions satisfies $|m - n| = 1$ [54–57].

In Figs. 5(a) and 5(b), we show the results of $\eta_s(\Omega)$ as a function of frequency Ω. When the disorder scattering is extremely small, $\eta_s(\Omega)$ shows a series of resonant

peaks as expected in Eq. (69). These peaks correspond to the transitions between the separated Landau levels. Meanwhile, the schematic diagrams, which can help us understand the transitions in Figs. 5(a) and 5(b) are given in Figs. 5(c) and 5(d). It can be seen from the numerical results combining with the schematic diagrams that the transitions between the same two Landau levels contributes the same intensity to the resonance peak of η_s despite the location of Fermi energy. The peaks T_1, T_3, and T_4 in Figs. 5(a) and 5(b) have same intensities since they correspond to the same transitions in two cases, as shown in Figs. 5(c) and 5(d). The peak T_2 in Fig. 5(b) is half of that in Fig. 5(a) because the peak T_2 in Fig. 5(a) contains the transitions E_{3-} to E_{1+} and E_{1-} to E_{3+} but the peak T_2 in Fig. 5(a) has only contributions from E_{1-} to E_{3+}.

Another notable feature in the analytic solution Eq. (69) is $\frac{n+1}{\Omega}$. For $\Omega > 0$, in the electron-hole (e-h) transitions, $\frac{n+1}{\Omega} \propto \Omega$ due to $\hbar\Omega = |E_{n+2,s'} - E_{ns}| \approx 2\sqrt{n}\hbar\omega_c$, but in the electron-electron (e-e) transitions, $\frac{n+1}{\Omega} \propto \Omega^{-3}$ since $\hbar\Omega = |E_{n+2,s'} - E_{ns}| \approx \frac{\hbar\omega_c}{\sqrt{n}}$. This is also confirmed by the numerical results in Fig. 5(b), where the η_s contributed by electron-electron transition tends to diverge as Ω approaches zero. As the Landau levels gradually overlap, the peak of $\eta_s(\Omega)$ will drop and merge with others, but as shown by the numerical results, the magnitude of η_s still maintains a general trend of decreasing with Ω for the e-e transitions and increasing with Ω for the e-h transitions.

B. Dynamic Hall viscosity $\eta_H(\Omega)$

The Kubo formula of dynamic Hall viscosity is similar as the one of the static shear viscosity except the finite frequency Ω. It is also divided into three parts as

$$
\eta_H(\Omega) = \text{Re}\left[\eta_H^{I,RA}(\Omega) - \eta_H^{I,RR}(\Omega) + \eta_H^{II}(\Omega) \right]. \quad (70)
$$

Then, we evaluate dynamic Hall viscosity at the well separated Landau levels region and zero temperature,

$$
\eta_H(\Omega) = \frac{\hbar^3 \omega_c^2}{8\pi l_B^2} \sum_{n,s,s'} \frac{n+1}{\Omega}
$$
$$
\times \left\{ 2(f_{E_{ns}+\Omega} - f_{E_{ns}}) \frac{\Omega - E_{n+2,s'} + E_{ns}}{(\Omega - E_{n+2,s'} + E_{ns})^2 + \Gamma^2} \right.
$$
$$
+ (f_{E_{n+2,s'}+\Omega} - f_{E_{ns}-\Omega}) \frac{\Omega + E_{n+2,s'} - E_{ns}}{(\Omega + E_{n+2,s'} - E_{ns})^2 + \Gamma^2}
$$
$$
\left. - (E_{ns} \leftrightarrow E_{n+2,s'}) \right\}, \quad (71)
$$

where the self-energy is assumed to be a small pure imaginary number $-i\Gamma$. It is obvious that, at the limit $\Omega \to 0$, the first and second terms in the curly brace represent the Fermi surface and Fermi sea contributions, which have been analyzed in the section of static Hall viscosity. Here, we focus on the dependence of η_H on Ω. Since the term $\frac{\Omega \mp E_{n+2,s'} \pm E_{ns}}{(\Omega \mp E_{n+2,s'} \pm E_{ns})^2 + \Gamma^2}$ in Eq. (71) describes a kink with the center $\Omega_c = \pm(E_{n+2,s'} - E_{ns})$, we assume the Ω in the distribution function multiplied by the kind function tends to Ω_c. Thus, the dynamic Hall
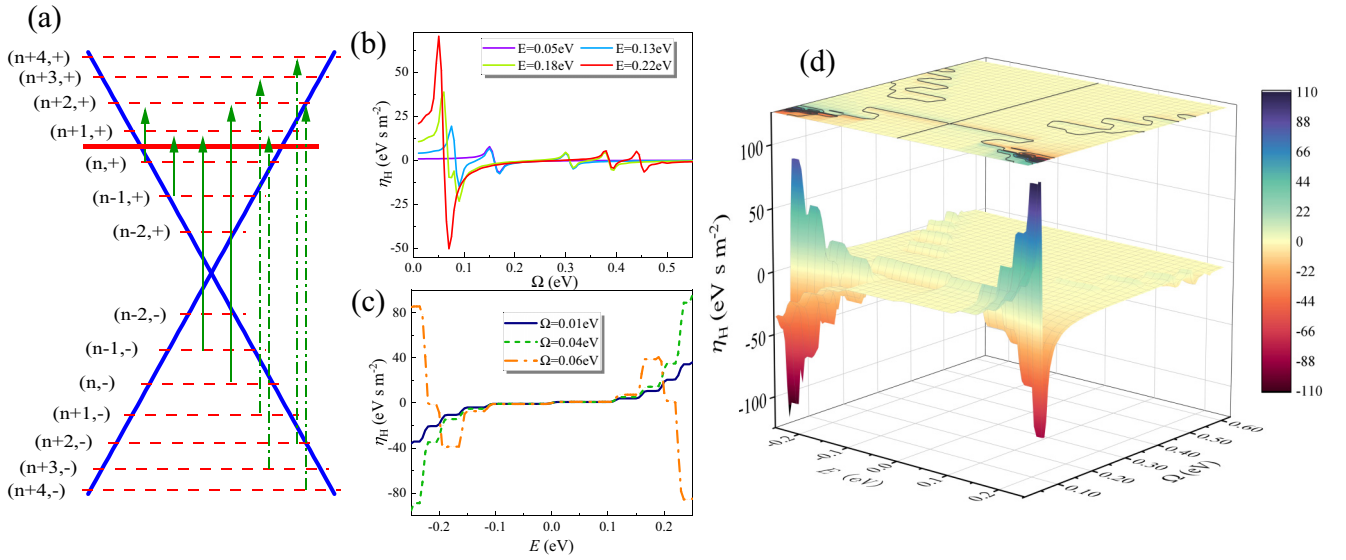
FIG. 6. (a) The schematic diagram of the allowed transitions in calculating dynamic Hall viscosity. (b) Dynamic Hall viscosity η_H vs frequency Ω for magnetic field $B = 10$ T and several Fermi energies. (c) Dynamic Hall viscosity η_H vs Fermi energy E for same magnetic field and several frequencies. (d) A global dependence of η_H on Ω and E.

viscosity can be further simplified as

$$
\eta_H(\Omega) \approx \frac{\hbar^3 \omega_c^2}{8\pi l_B^2} \sum_{n,s,s'} \frac{n+1}{\Omega}
$$
$$
\times \left[(f_{E_{n+2,s'}} - f_{E_{ns}}) \frac{\Omega - E_{n+2,s'} + E_{ns}}{(\Omega - E_{n+2,s'} + E_{ns})^2 + \Gamma^2} \right.
$$
$$
\left. - (E_{ns} \leftrightarrow E_{n+2,s'}) \right]. \tag{72}
$$

This expression is somewhat analogous to the evaluation of dynamic shear viscosity in the well separated Landau levels region Eq. (69). They have the same transition rule $n \leftrightarrow n + 2$, but different types of transition function: delta structure for $\eta_s(\Omega)$ and kink structure for $\eta_H(\Omega)$. Another essential different between these two is the sign before the exchange ($E_{ns} \leftrightarrow E_{n+2,s'}$). In the expression of $\eta_s(\Omega)$, it is a plus sign, which means the addition of the counterparts. In the expression of $\eta_H(\Omega)$, however, it is a minus sign, so the counterparts cancel each other out. Figure 6(a) shows the schematic diagram of the transitions in a general case where the Fermi level is assumed to fall in the gap between the Landau levels with indices $(n, +)$ and $(n + 1, +)$. It is noticeable that there are only four transitions left, as the others cancel out with their counterparts under the exchange $(ns) \leftrightarrow (n + 2, s')$.

The numerical results of dynamic Hall viscosity are shown in Figs. 6(b)–6(d). In Fig. 6(b), we plot dynamic Hall viscosity η_H versus frequency Ω in the presence of magnetic field $B = 10$ T. The energies of the low-order Landau levels in this condition are shown in Figs. 5(c) and 5(d). For Fermi energy $E = 0.05$ eV, there is only one resonance kink structure around $\Omega = 0.16$ eV, which is consistent with the prediction of Eq. (72), since there is only one single transition with frequency $\Omega = 0.16$ eV in this case. For Fermi energy $E = 0.13$ eV, there are three resonance kink structures corresponding to the three single transitions at $\Omega = 0.09$ eV,

0.16 eV, and 0.31 eV. For Fermi energy $E = 0.18$ eV and 0.22 eV, there should be four resonance kink structures according to the Eq. (72). However, in the numerical results, the lowest two resonance structure are partially and fully overlap for $E = 0.18$ eV and $E = 0.22$ eV, since their transition frequencies are too close together.

In Fig. 6(b), we plot η_H versus E for different frequencies. In Fig. 6(b), we plot a global dependence of η_H on Ω and E. Both of these figures show how the static quantized Hall viscosity should evolve into the dynamic Hall viscosity. The plateau structure is retained, but the heights of the plateaus vary with frequency and resonate around the frequencies that lead to single transitions.

V. DISCUSSION

We have presented a microscopic theory on hydrodynamic electrons in disordered graphene. We provide a unified description for both undoped and doped graphene, with or without external magnetic fields. Surprisingly, we identify the shear viscosity exhibits an anomalous enhancement around the Dirac point, due to disorder-assisted electron-hole collisions, in remarkable contrast to the normal Fermi liquids. Interestingly, by considering the external magnetic field, the shear viscosity can be further enhanced. Additionally, it is found that the anomalous change of viscosity can be also revealed in the dynamic and magneto-hydrodynamic responses.

Our findings reveal that the impurities offer a counterintuitive effect on the collective motion of electrons in graphene near the Dirac point, due to electron-hole collisions that do not exist in conventional 2DEG. It implies that undoped graphene is nice to realize hydrodynamic electronics. Moreover, momentum currents contain single-particle contributions compared to charge currents, which makes the disorder-assisted effect significantly larger in viscosity than in conductivity. Uncovering the critical relevance of hydrodynamic electronics with electron-hole coherent collisions

affords a unique link between quantum-critical electron transport and the wealth of fluid dynamics phenomena.

The current paper is complementary to the existing studies on electron viscosity. Generally speaking, the effect of impurities is believed to suppress the scattering events with small momentum transfer [58] and collective motion of electrons [59]. Here, our findings demonstrate that the effect of impurities on the viscosity in graphene needs a careful study, especially around the Dirac point, where the density of states can be enhanced by impurities.

Furthermore, electrons in graphene behave as quasirelativistic gas of quasiparticles satisfying the relativistic equation of motion, providing a playground to study relativistic effects in fluid dynamics. In this paper, we have shown that the electron-hole coherence related to quasirelativistic nature of graphene results in numerous peculiar behaviors in both static and dynamic viscosities. It calls for more careful studies on the Navier-Stokes equation due to relativistic effects in describing the flow of Dirac electrons.

[1] R. N. Gurzhi, Minimum of resistance in impurity-free conductors, JETP **17**, 521 (1963).

[2] D. A. Bandurin, I. Torre, R. K. Kumar, M. B. Shalom, A. Tomadin, A. Principi, G. H. Auton, E. Khestanova, K. S. Novoselov, I. V. Grigorieva et al., Negative local resistance caused by viscous electron backflow in graphene, Science **351**, 1055 (2016).

[3] D. A. Bandurin, A. V. Shytov, L. S. Levitov, R. K. Kumar, A. I. Berdyugin, M. B. Shalom, I. V. Grigorieva, A. K. Geim, and G. Falkovich, Fluidity onset in graphene, Nat. Commun. **9**, 4533 (2018).

[4] R. Krishna Kumar, D. A. Bandurin, F. M. D. Pellegrino, Y. Cao, A. Principi, H. Guo, G. H. Auton, M. B. Shalom, L. A. Ponomarenko, G. Falkovich et al., Superballistic flow of viscous electron fluid through graphene constrictions, Nat. Phys. **13**, 1182 (2017).

[5] H. Guo, E. Ilseven, G. Falkovich, and L. S. Levitov, Higher-than-ballistic conduction of viscous electron flows, Proc. Natl. Acad. Sci. USA **114**, 3068 (2017).

[6] A. C. Keser, D. Q. Wang, O. Klochan, Derek Y. H. Ho, O. A. Tkachenko, V. A. Tkachenko, D. Culcer, S. Adam, I. Farrer, D. A. Ritchie, O. P. Sushkov, and A. R. Hamilton, Geometric Control of Universal Hydrodynamic Flow in a Two-Dimensional Electron Fluid, Phys. Rev. X **11**, 031030 (2021).

[7] L. Levitov and G. Falkovich, Electron viscosity, current vortices and negative nonlocal resistance in graphene, Nat. Phys. **12**, 672 (2016).

[8] J. Mayzel, V. Steinberg, and A. Varshney, Stokes flow analogous to viscous electron current in graphene, Nat. Commun. **10**, 937 (2019).

[9] G. Falkovich and L. Levitov, Linking Spatial Distributions of Potential and Current in Viscous Electronics, Phys. Rev. Lett. **119**, 066601 (2017).

[10] J. A. Sulpizio, L. Ella, A. Rozen, J. Birkbeck, D. J. Perello, D. Dutta, M. Ben-Shalom, T. Taniguchi, K. Watanabe, T. Holder et al., Visualizing Poiseuille flow of hydrodynamic electrons, Nature (London) **576**, 75 (2019).

[11] P. J. W. Moll, P. Kushwaha, N. Nandi, B. Schmidt, A. P. Mackenzie, Evidence for hydrodynamic electron flow in PdCoO₂, Science **351**, 1061 (2016).

[12] A. I. Berdyugin, S. G. Xu, F. M. D. Pellegrino, R. K. Kumar, A. Principi, I. Torre, M. B. Shalom, T. Taniguchi, K. Watanabe, I. V. Grigorieva et al., Measuring Hall viscosity of graphene's electron fluid, Science **364**, 162 (2019).

[13] J. Crossno, J. K. Shi, K. Wang, X. Liu, A. Harzheim, A. Lucas, S. Sachdev, P. Kim, T. Taniguchi, K. Watanabe et al., Observation of the Dirac fluid and the breakdown of the Wiedemann-Franz law in graphene, Science **351**, 1058 (2016).

[14] J. Gooth, F. Menges, N. Kumar, V. Süß, C. Shekhar, Y. Sun, U. Drechsler, R. Zierold, C. Felser and B. Gotsmann, Thermal and electrical signatures of a hydrodynamic electron fluid in tungsten diphosphide, Nat. Commun. **9**, 4093 (2018).

[15] U. Briskot, M. Schütt, I. V. Gornyi, M. Titov, B. N. Narozhny, and A. D. Mirlin, Collision-dominated nonlinear hydrodynamics in graphene, Phys. Rev. B **92**, 115426 (2015).

[16] M. Müller, J. Schmalian, and L. Fritz, Graphene: A Nearly Perfect Fluid, Phys. Rev. Lett. **103**, 025301 (2009).

[17] B. N. Narozhny and M. Schütt, Magnetohydrodynamics in graphene: Shear and Hall viscosities, Phys. Rev. B **100**, 035125 (2019).

[18] I. Torre, A. Tomadin, A. K. Geim, and M. Polini, Nonlocal transport and the hydrodynamic shear viscosity in graphene, Phys. Rev. B **92**, 165433 (2015).

[19] F. M. D. Pellegrino, I. Torre, A. K. Geim, and M. Polini, Electron hydrodynamics dilemma: Whirlpools or no whirlpools, Phys. Rev. B **94**, 155414 (2016).

[20] A. Lucas, Hydrodynamic transport in strongly coupled disordered quantum field theories, New J. Phys. **17**, 113007 (2015).

[21] A. Lucas and K. C. Fong, Hydrodynamics of electrons in graphene, J. Phys.: Condens. Matter **30**, 053001 (2018).

[22] K. S. Novoselov et al. Two-dimensional gas of massless Dirac fermions in graphene, Nature (London) **438**, 197 (2005).

[23] M. Titov, Impurity-assisted tunneling in graphene, Europhys. Lett. **79**, 17004 (2007).

[24] K. Nomura and A. H. MacDonald, Quantum Transport of Massless Dirac Fermions, Phys. Rev. Lett. **98**, 076602 (2007).

[25] S. Adam, E. H. Hwang, V. M. Galitski, and S. Das Sarma, A self-consistent theory for graphene transport, Proc. Natl. Acad. Sci. USA **104**, 18392 (2007).

[26] I. S. Burmistrov, M. Goldstein, M. Kot, V. D. Kurilovich, and P. D. Kurilovich, Dissipative and Hall Viscosity of a Disordered 2D Electron Gas, Phys. Rev. Lett. **123**, 026804 (2019).

[27] P. S. Alekseev, Negative Magnetoresistance in Viscous Flow of Two-Dimensional Electrons, Phys. Rev. Lett. **117**, 166601 (2016).

[28] F. M. D. Pellegrino, I. Torre, and M. Polini, Nonlocal transport and the Hall viscosity of two-dimensional hydrodynamic electron liquids, Phys. Rev. B **96**, 195401 (2017).

[29] L. Hu, Z. Liu, D. N. Sheng, F. D. M. Haldane, and W. Zhu, Microscopic diagnosis of universal geometric responses in fractional quantum Hall liquids, Phys. Rev. B **103**, 085103 (2021).

[30] J. E. Avron, Odd viscosity, J. Stat. Phys. **92**, 543 (1998).

[31] B. Bradlyn, M. Goldstein, and N. Read, Kubo formulas for viscosity: Hall viscosity, Ward identities, and the relation with conductivity, Phys. Rev. B **86**, 245309 (2012).

[32] M. Sherafati, A. Principi, and G. Vignale, Hall viscosity and electromagnetic response of electrons in graphene, Phys. Rev. B **94**, 125427 (2016).

[33] O. H. Nielsen and R. M. Martin, Quantum-mechanical theory of stress and force, Phys. Rev. B **32**, 3780 (1985).

[34] P. K. Kundu and I. M. Cohen, *Fluid Mechanics*, Fourth Edition (Elsevier, Amsterdam, 2008).

[35] Y. B. Band and Y. Avishai, *Quantum Mechanics with Applications to Nanotechnology and Information Science* (Academic Press, New York, 2013).

[36] N. Read and E. H. Rezayi, Hall viscosity, orbital spin, and geometry: Paired superfluids and quantum Hall systems, Phys. Rev. B **84**, 085316 (2011).

[37] L. D. Landau and E. M. Lifshitz, *Theory of Elasticity*, Second edition (Elsevier, Amsterdam, 1970).

[38] D. N. Blaschke, R. Gieres. M. Reboud, and M. Schweda, The energy-momentum tensor(s) in classical gauge theories, Nucl. Phys. B **912**, 192 (2016).

[39] A. F. Palacios, *The Hamilton-Type Principle in Fluid Dynamics* (Springer, Vienna, 2006).

[40] J. M. Link, D. E. Sheehy, B. N. Narozhny, and J. Schmalian, Elastic response of the electron fluid in intrinsic graphene: The collisionless region, Phys. Rev. B **98**, 195103 (2018).

[41] P. Rao and B. Bradlyn, Hall Viscosity in Quantum Systems with Discrete Symmetry: Point Group and Lattice Anisotropy, Phys. Rev. X **10**, 021005 (2020).

[42] Proof of symmetry of $\mathcal{J}'_{ij}$: $\mathcal{J}'_{ij} - \mathcal{J}'_{ji} = -(x_i p_j - x_j p_i) - \frac{i\hbar}{4}[\sigma_i, \sigma_j] = -\varepsilon^{ijk} L_k + \varepsilon^{ijk}\frac{\hbar}{2}\sigma_k = 0$, since the pseudospin of graphene is commonly thought to be analogous to a spin-1/2 angular momentum.

[43] V. A. Zakharov and I. S. Burmistrov, Residual bulk viscosity of a disordered two-dimensional electron gas, Phys. Rev. B **103**, 235305 (2021).

[44] See Supplemental Material at http://link.aps.org/supplemental/10.1103/PhysRevB.106.014205 for detailed derivations.

[45] G. D. Mahan *Many-Particle Physics* (Springer, Berlin, 2000).

[46] H. Bruus and K. Flensberg, *Many-Body Quantum Theory in Condensed Matter Physics* (Oxford University Press, New York, 2004).

[47] W. Zhu, Q. W. Shi, X. R. Wang, X. P. Wang, J. L. Yang, J. Chen, and J. G. Hou, Evaluation of the Green's function of disordered graphene, Phys. Rev. B **82**, 153405 (2010).

[48] B. Sbierski, K. A. Madsen, P. W. Brouwer, and C. Karrasch, Quantitative analytical theory for disordered nodal points, Phys. Rev. B **96**, 064203 (2017).

[49] A. M. Martin, G. Litak, B. L. Györffy, J. F. Annett, and K. I. Wysokiński, Coherent potential approximation for *d*-wave superconductivity in disordered systems, Phys. Rev. B **60**, 7523 (1999).

[50] P. M. Ostrovsky, I. V. Gornyi, and A. D. Mirlin, Electron transport in disordered graphene, Phys. Rev. B **74**, 235443 (2006).

[51] W. Chen, Y. Shen, B. Fu, Q. Shi, W. Zhu, On the sample-dependent minimal conductivity in weakly disordered graphene, arXiv:2108.13787.

[52] C. Hoyos and D. T. Son, Hall Viscosity and Electromagnetic Response, Phys. Rev. Lett. **108**, 066805 (2012).

[53] S. Das Sarma, S. Adam, E. H. Hwang, and E. Rossi, Electronic transport in two-dimensional graphene, Rev. Mod. Phys. **83**, 407 (2011).

[54] V. P. Gusynin, S. G. Sharapov, and J. P. Carbotte, Unusual Microwave Response of Dirac Quasiparticles in Graphene, Phys. Rev. Lett. **96**, 256802 (2006).

[55] V. P. Gusynin and S. G. Sharapov, Transport of Dirac quasiparticles in graphene: Hall and optical conductivities, Phys. Rev. B **73**, 245411 (2006).

[56] V. P. Gusynin, S. G. Sharapov and J. P. Carbotte, Magnetooptical conductivity in graphene, J. Phys.: Condens. Matter **19**, 026222 (2007).

[57] V. P. Gusynin, S. G. Sharapov, and J. P. Carbotte, Anomalous Absorption Line in the Magneto-Optical Response of Graphene, Phys. Rev. Lett. **98**, 157402 (2007).

[58] A. Principi, G. Vignale, M. Carrega, and M. Polini, Bulk and shear viscosities of the two-dimensional electron liquid in a doped graphene sheet, Phys. Rev. B **93**, 125410 (2016).

[59] M. Polini and A. Geim, Viscous electron fluids, Phys. Today **73**, 28 (2020).